Analytica Chimica Acta 1376 (2025) 344607

Contents lists available at ScienceDirect

Analytica Chimica Acta

journal homepage: www.elsevier.com/locate/aca

Enhancing *in-situ* molecular profiling of gastric cancer for spatial proteomics through optimized digestion

Lydia Jung [a], Julius Shakhtour [a], Bianca Grosser [a,b], Gisela Keller [a], Tanja Groll [a], Margaret Tulessin [a], Claire Delbridge [a], Kristina Schwamborn [a], Juliana P.L. Gonçalves [a,*]

[a] *Institute of Pathology, School of Medicine and Health, Technical University of Munich, Trogerstraße 18, 81675, Munich, Germany*
[b] *Pathology, Medical Faculty Augsburg, University of Augsburg, Augsburg, Germany*

HIGHLIGHTS

- An optimized enzymatic digestion protocol for MALDI-MSI improved gastric cancer tissue analysis.
- MALDI-MSI revealed molecular differences linked to tumor progression and treatment response.
- Potential biomarkers for gastric cancer prognosis and stratification were identified.
- Findings support the need for tissue-specific digestion protocols in clinical proteomics.

GRAPHICAL ABSTRACT

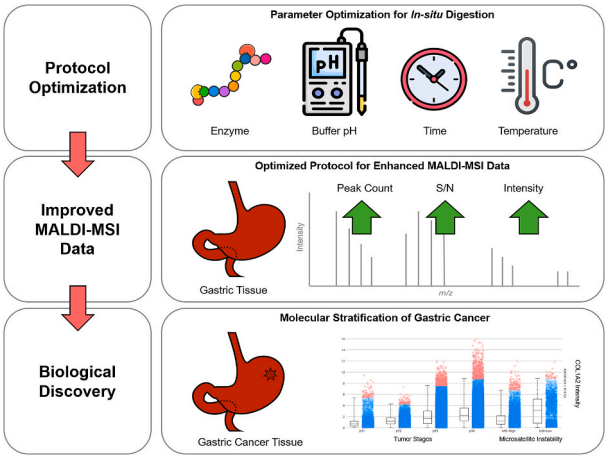

ARTICLE INFO

Handling Editor: Dr. L. Liang

Keywords:
Mass spectrometry imaging
In-situ proteomics
Gastric cancer
Translational mass spectrometry

ABSTRACT

Background: Gastric cancer has a high incidence worldwide, affecting men more frequently than women. Treatment options remain limited in their success, primarily due to insufficient knowledge about the disease. The high degree of heterogeneity in gastric tissue can obscure molecular information, making comprehensive analysis challenging. Enzymatic digestion, a crucial step in protein analysis, is not yet sufficiently optimized for specific human tissue samples like gastric tissue, thereby limiting the analytical potential of techniques such as matrix-assisted laser desorption/ionization - mass spectrometry imaging (MALDI-MSI).
Results: We utilized archived specimens from 103 patient-derived samples across nine tissue types (brain, breast, kidney, lung, liver, pancreas, stomach, tonsil, and leiomyoma) to test different protocols aiming to improve tryptic digestion of formalin-fixed, paraffin-embedded tissues for *in-situ* proteomic analysis. The optimized digestion protocol improved peptide detection and spectral quality while preserving histological integrity. This

This article is part of a special issue entitled: Imaging Mass Spectrometry published in Analytica Chimica Acta.

* Corresponding author.
E-mail address: juliana.goncalves@tum.de (J.P.L. Gonçalves).

https://doi.org/10.1016/j.aca.2025.344607
Received 12 May 2025; Received in revised form 6 August 2025; Accepted 3 September 2025
Available online 4 September 2025

protocol was employed to characterize a gastric cancer cohort (N = 97). MALDI-MSI data identified molecular signatures associated with disease progression, microsatellite instability status, treatment response, and spatial distribution.

Significance: We gained access to molecular information on tumor progression and treatment response by employing a tailored tryptic digestion protocol for MALDI-MSI detection. By advancing molecular profiling in gastric cancer, these findings provide valuable insight into disease-related molecular changes and contribute to developing more precise and personalized diagnostic strategies.

1. Introduction

According to the Global Cancer Organization, in 2022 alone, there were nearly a million new cases of gastric cancer (GC), and over 660000 deaths were reported worldwide [1]. GC treatment and prognosis are largely determined by the cancer's stage, primarily assessed using the American Joint Committee on Cancer tumor-node-metastasis (TNM) system. This system evaluates three key aspects: the extent of tumor invasion into gastric wall layers (T category), the spread to regional lymph nodes (N category), and the presence of cancer cells in other organs (M category). The TNM information is combined to assign an overall stage, ranging from 0 (carcinoma *in situ*) to IV, with higher numbers indicating more advanced cancer and greater extent of spread. Surgery is the primary treatment approach for all stages, especially early-stage GC. Chemotherapy or chemoradiation is used either before surgery to shrink tumors or after surgery to eliminate remaining cancer cells. For advanced GC patients with unresectable, recurrent, or metastatic cancer, chemotherapy is typically the first-line treatment to control cancer progression and may be combined with targeted therapy, immunotherapy, or radiation therapy [2].

Matrix-Assisted Laser Desorption/Ionization Mass Spectrometry Imaging (MALDI-MSI) has become an important tool in translational research, enabling detailed molecular-level analysis of biological tissues [3,4]. This technique combines mass spectrometry with spatial mapping, facilitating visualization of biomolecules like proteins or peptides within tissue sections [5,6].

MALDI-MSI preserves sample structural integrity, making it exceptional for exploring complex biological systems and disease pathology [7]. It offers deeper insights into tissue composition, enhancing differential diagnoses and aiding in distinguishing cancer subtypes [8,9].

Despite advances in multimodal treatment strategies, GC remains a highly heterogeneous disease with a poor prognosis, highlighting the need for improved molecular characterization. Traditional histopathological methods, such as immunohistochemistry (IHC) and genomic sequencing, provide valuable insights but may not fully capture the complexity of GC at the molecular level [10,11].

Patient GC samples for this study stem from a real-world cohort of patients undergoing treatment with neoadjuvant chemotherapy (CTx) utilizing platinum/fluoropyrimidine, with or without the addition of a taxane-containing compound. Microsatellite instability (MI) was proposed as a vital prognostic factor, particularly when analyzed together with gender and treatment regimens [12]. Given GC's complexity, a systematic approach to optimizing MALDI-MSI protocols is essential to enhance molecular profiling and improve diagnostic accuracy.

Formalin-fixed paraffin-embedded (FFPE) tissue fixation is the gold standard in histopathology and clinical diagnostics, offering a long-term, durable, and cost-effective preservation method compared to frozen tissue [13,14]. Several analytical approaches, such as IHC, RNA, and DNA sequencing, have FFPE compatible protocols. MALDI-MSI sample preparation procedures have also been specifically developed for FFPE tissues [15–18]. Enzymatic digestion is critical for peptide/-protein analysis, with each tissue type presenting unique biochemical and morphological challenges that affect digestion efficiency, ionization, and molecular detection [13,19–22].

Consequently, optimized protocols are necessary for studies focusing on tissues of one specific origin.

To address these challenges, this study systematically evaluates digestion conditions, such as temperature, buffer pH, and incubation times, across diverse tissue types to establish optimal MALDI-MSI parameters for GC *in situ* proteomic analysis. A tissue microarray (TMA) containing nine tissue types - brain, breast, kidney, lung, liver, pancreas, gastric, tonsil, and leiomyoma - was analyzed under various preparation conditions. Based on the outcome, an optimized digestion protocol was developed specifically for gastric tissue and applied to a GC cohort. Given GC's complex histology and high mortality rate, improved molecular characterization could provide valuable insights into its pathophysiology and aid in developing more precise diagnostic and therapeutic strategies [10,23].

2. Materials and methods

2.1. Patient cohort

A TMA (TMA A) with archival tissues from different organs was utilized for the protocol optimization. 1 mm diameter cores of lung (N = 10), breast (N = 10), pancreas (N = 12), liver (N = 10), kidney (N = 9), leiomyoma (N = 14), tonsil (N = 11), brain (N = 10), and stomach (N = 18) were randomly arranged in a paraffin block.

The archive of the Institute of Pathology of the Technical University of Munich was also searched for GC patients treated with a platinum/fluoropyrimidine neoadjuvant CTx without or with taxane between 1994 and 2018. In total, 394 patients were included in a previous study from which our study cohort was derived [12]. For this study, we used four TMAs (TMAs B-E, N = 97), each containing samples from 24 to 25 patients. For each patient, three replicates were included to increase tumor representativeness. Of the 20 female patients, ten showed a partial treatment response (one with high microsatellite instability (MI-high)), while the others did not respond (three MI-high, the others were microsatellite stable (MSS)). Among 77 male patients, 38 partially responded (two MI-low, 36 MSS), while non-responders included five MI-high, one MI-low, and 33 MSS (Fig. 1). Clinical information, such as tumor localization and pathological T (pT)-status, within the TNM staging system for cancer was retrieved from the database of the Institute of Pathology and added as attributes to the mass spectrometry data, which was conducted according to the recommendations by the Union for International Cancer Control (UICC), 7th edition (UICC, 2010) [23,24]. The study was approved by the institutional ethics review board (Ethics Committee of the Technical University of Munich Faculty of Medicine, Protocol Number 502/15s).

2.2. Sample preparation

TMA sections (4 μm) were mounted onto indium-tin-oxide slides (Bruker Daltonics GmbH & Co. KG, Bremen, Germany) coated with 0.1 % Poly-L-lysine (Sigma-Aldrich. Merck KGaA, Darmstadt, Deutschland). The slides were then dried in an oven at 37 °C for at least 3 h and stored in a low humidity environment at room temperature (RT) until further use.

Sample preparation was based on a previously published protocol [21]. Briefly, the tissue sections were deparaffinized in an oven (VWR International, Darmstadt, Germany; DRY-Line 53), at 80 °C for 15 min, followed by two 100 % xylene and one isopropanol washes. Rehydration

was done by graded ethanol washes (100 %, 95 %, 70 %, 50 %) for 5 min each. The slides were then rinsed with ultra-pure water (5 s) and dried under vacuum for 10 min. Antigen retrieval was performed by heating slides in a decloaking chamber (BioCare Medical, Pacheco, CA, USA) with ultra-pure water at 110 °C for 20 min. The slides were cooled to RT and dried in the desiccator. For the digestion, optimization of the individual parameters was carried in individual experiments, as summarized in Table 1.

Different enzyme solutions were compared to sequencing grade modified trypsin (Promega GmbH, Walldorf, Germany, V5111) prepared in a 20 mM ammonium bicarbonate buffer with 0.01 % glycerol. Trypsin Platinum (Promega GmbH, VA900A) was resuspended by dissolving 100 µg lyophilized enzyme in 2 mL deionized water with 0.0125 % glycerol (Sigma-Aldrich). Aliquots (400 µL) were stored at −20 °C and diluted in 400 µL of 40 mM ammonium bicarbonate buffer before use. Trypsin SOLu (Sigma-Aldrich, EMS0004) was prepared by adding 20 µL of stock solution (100 µg/mL) to 780 µL of 20 mM ammonium bicarbonate (Sigma-Aldrich) buffer with 0.01 % glycerol. Trypsin/Lys-C Mix (Promega GmbH, V507A) was prepared similarly to standard trypsin, maintaining a final enzyme concentration of 25 µg/mL. For pepsin (Promega GmbH, V195A), the concentration was changed to 1 mg/mL, as used in previous studies and recommended by the supplier [25,26]. A pH 2 buffer containing ultra-pure water with 0.05 % trifluoroacetic acid (TFA, Sigma-Aldrich) was prepared. The enzyme was resuspended in ultra-pure water with 0.0125 % glycerol. Aliquots (200 µL) were stored at 4 °C before use. 600 µL of pH 2 buffer was added at the time of digestion.

To compare the impact of different pH, ammonium bicarbonate buffers were adjusted to pH 7.4 and pH 8.9 by adding 96 % acetic acid (Carl Roth GmbH & Co. KG, Karlsruhe, Germany) or 28 % ammonium hydroxide (Sigma-Aldrich), respectively. Aliquots (200 µL) were stored at −20 °C.

The enzyme solutions were sprayed, using an automated spraying device (TM Sprayer, HTX Technologies, Chapel Hill, NC, USA), onto tissue sections of TMA A in a criss-cross pattern with a track spacing of 2 mm and velocity of 750 mm/min. A total of 16 layers were deposited under a controlled nitrogen flow (10 psi) at 30 °C.

Table 1
Experimental parameters with corresponding changes for enzymatic digestion optimization. *Solely used for pepsin.

Standard Enzymatic Digestion Parameters [21]			
Enzyme	Buffer pH	Incubation time	Incubation temperature
Trypsin Sequencing grade	pH 8.4	2 h	50 °C
Adjusted Parameters for Optimization			
Trypsin Platinum	pH 7.4	1 h	RT
Trypsin/Lys-C	pH 8.9	4 h	37 °C
Trypsin SOLu		Overnight	
Pepsin	pH 2.0*		

Following enzyme application, the slides were incubated in a digestion chamber with saturated K_2SO_4 (Carl Roth GmbH & Co. KG) aqueous solution to ensure a controlled humidity environment. Teaching marks were drawn on the slides and scanned at 1200 dpi for positional teaching in flexControl (v.4.2) and flexImaging. α-cyano-4-hydroxycinnamic acid (HCCA, Sigma-Aldrich) matrix (10 mg/mL in 70 % acetonitrile with 1 % TFA) was sprayed in four layers in a heel-to-heel pattern at 1200 mm/min at a flow of 120 µL/min at 75 °C and 3 mm track spacing under 10 psi nitrogen flow onto the slides using a liquid chromatography pump and TM sprayer ≥ 99.9 % reagent grade or HPLC grade unless otherwise specified. In each experiment, a slide was prepared according to the standard protocol to allow for direct comparison. To ensure reproducibility and rule out accidental findings, all experiments were repeated at least twice.

Following the initial set of experiments, the most promising conditions, based on the peak count, top 50 peak list, and S/N, were selected for optimizing the digestion of gastric tissue. Changes to the protocol were implemented and are summarized in Table 2.

For GC tissue typing, the TMAs B-E were prepared based on the parameters of optimization 3, as it resulted in the best peak count, S/N, and peak intensities.

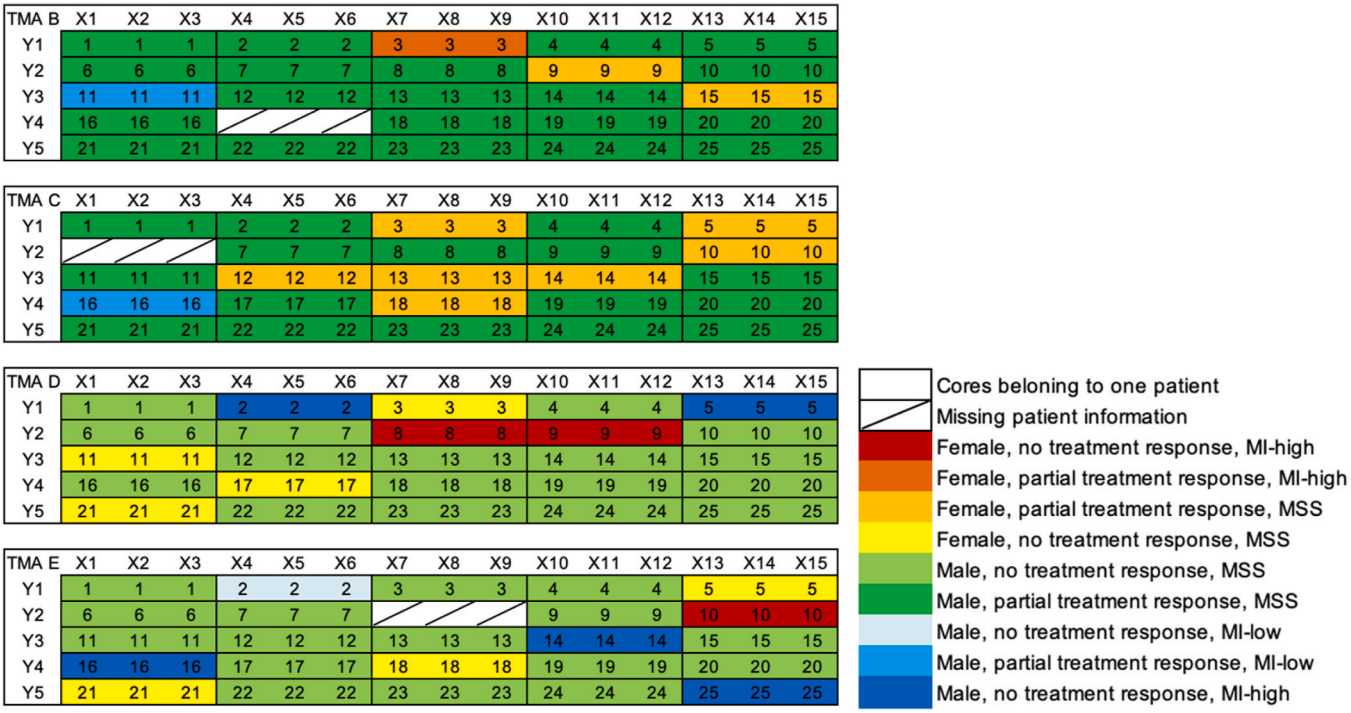

Fig. 1. Layout of the GC TMAs B to E with corresponding information about the patient regarding gender, treatment response, and microsatellite instability.

Table 2
Experimental setups for the individual optimization experiments 1 to 3, with corresponding parameter adaptation, and the standard protocol [21].

Optimization Experiments			
Optimization 1	Optimization 2	Optimization 3	Standard
Trypsin SOLu	Trypsin SOLu	Trypsin Sequencing Grade	Trypsin Sequencing Grade
pH 8.9 37 °C 1 h	pH 8.9 37 °C 2 h	pH 8.9 37 °C 2 h	pH 8.4 50 °C 2 h

2.3. MALDI-TOF acquisition

MALDI-MSI data was acquired on a rapifleX MALDI Tissue-typer mass spectrometer (Bruker Daltonics GmbH & Co. KG) in positive-ion reflector mode across a mass range of *m/z* 599–3201.

Mass calibration was performed using the peptide calibration standard II (Bruker Daltonics).

For acquisition, 500 laser shots at 10 kHz, with smartbeam M5 small laser settings, were used with an effective field size of 50x50 μm. Laser power was set to approximately 75 %, and adjusted to achieve comparable signal intensity for all samples. The sample rate was set at 1.25 GS/s, and realtime smoothing was disabled to maintain data integrity. The global offset attenuator was set to 5 %.

MALDI-TOF parameters remained consistent across experiments to ensure comparability. For pepsin digestion (200 μg/mL), the measurement range was adjusted to *m/z* 499–3201 due to smaller protein fragments and cleavage at hydrophobic and aromatic residues [27]. Following data acquisition, the matrix was removed by washing the slides with methanol (99.5 %, Carl Roth GmbH & Co. KG) for 30 s and ethanol for 30 s. Hematoxylin and eosin (H&E) staining was performed once per experimental setup to assess tissue morphology and quality.

Microscopic images were acquired using an Aperio AT2 DX System slide scanner (Leica Biosystems, Wetzlar, Germany) and analyzed by a pathologist (J.S.). Digestion damage to the tissue was graded as follows: 0 = no visible damage, 1 = slight damage with no physiological impact, 2 = damage with recognizable components, and 3 = severely damaged. Cumulative scores for each tissue type were calculated by summing individual core ranks independent of core count (equations (1)–(3)). For gastric tissue optimization and GC typing, only equations (1) and (2) were utilized.

$$\text{Damage score per core } [\%] = \frac{\text{score}}{3} \times 100 \quad [1]$$

$$\%\text{damage by tissue} = \frac{\sum \text{damage per core}}{\text{total nr. of cores of tissue}} \times 100 \quad [2]$$

$$\%\text{tissue specific damage} = \frac{\sum \text{damage score}}{\text{total cores TMA}} \times 100 \quad [3]$$

2.4. Feature identification

Peptides resulting from area under the curve-receiver operating characteristic (AUC-ROC) analysis (below 0.3 or above 0.7) were determined as differentiating features. To identify the differentiating features, we attempted on tissue MS/MS detection utilizing one whole mount section of a patient included in the GC cohort. MS/MS was performed using a trapped ion mobility (tims)-TOF/TOF spectrometer (Bruker Daltonics GmbH & Co. KG) in positive ion mode. Sample preparation was carried out as described before, with the exception of red phosphorus (Bruker Daltonics GmbH & Co. KG) being used as mass calibrant. Laser power for fragmentation was set at 80 % and a beam scan of 20 μm^2. 1000 laser shots at a frequency of 10 kHz were acquired per spectrum, adjusting the transfer time, pre-pulse storage, collision energy, and RF depending on the peptide precursor ion. MS/MS spectra were deconvoluted using *MASCOT* [28] for protein identification. Peptide mass tolerance was defined as ±1 %, and fragment mass tolerance was set at ±0.8 Da, with a maximum of one missed cleavage allowed. Taxonomy was set to *homo sapiens* and the database searched was SwissProt. For the fragments that could not be isolated directly from the tissue, tentative identification was done based on previously reported peptide fragments (Table A. 3).

2.5. Data analysis

MALDI-MSI data was loaded in SCiLS Lab Pro (version 2024b, Bruker Daltonics GmbH & Co. KG) for data analysis. Pre-processing included baseline correction, mass alignment, and normalization of total ion count (TIC) [29].

Non-tissue regions were included in all measurements to account for potential error during matrix spraying or signal loss during data acquisition. K-means clustering was used to assess robustness of the acquire data with consistent clustering patterns visible across the different measurements. To assess potential batch effects and data comparability, principal component analysis (PCA) and clustering were performed (Figure A. 1 and A. 2). PCA used Pareto scaling, which was conducted on all individual spectra from tissue regions with weak denoising. Clustering was based on bisecting k-means with a correlation distance approach.

Three comparisons were made between experiments: average top 50 peak intensity, peak count, and S/N. Additionally, the autodigestion peaks of trypsin were compared. Distribution of the data was assessed using the Anderson-Darling test. Due to non-normal distribution of the data, statistical significance between groups was determined using the non-parametric Wilcoxon rank-sum test (Mann-Whitney U test).

Peak count indicated the number of detectable analytes in tissue, with peaks counted in the *m/z* 800–1100 mass range. Peaks in higher mass ranges were excluded to avoid automatic detection of background peaks by SCiLS. The “feature finding” tool in SCiLS Lab Pro was applied to TIC-normalized data, selecting 100 peaks per every 16th spectrum from every dataset. The peak list was exported, and peaks in the 800–1100 *m/z* range were counted in Excel.

The S/N was compared for the *m/z* 1105.59 peak, since it was consistently present and easily distinguishable from background noise. The background noise intensity was estimated from adjacent peaks. The 50 most intense monoisotopic peaks from the standard measurements were compared to evaluate digestion and detection efficiency. A comprehensive peak list, including all detected peaks, was generated using SCiLS Lab Pro and divided into six mass ranges. The number of features selected from each mass range was determined based on their distribution in the overall average spectrum, ensuring a balanced and representative selection across the mass ranges. The highest monoisotopic peaks from each section (*m/z* 600–1000; 1000–1400; 1400–1650; 1650–1900; 1900–2500; 2500–3200) were selected for the top 50 peak list (Table A. 1). Differences in average intensities throughout all experiments were statistically compared, e.g., using boxplots to show the average and median intensity of all 50 peaks as well as their distribution. The peaks *m/z* 842.51 and 2211.51, corresponding to trypsin autodigestion products, were used to assess enzymatic activity under the different experimental conditions [30]. For each peak, the S/N was calculated based on its relative intensity.

For the GC cohort, clinical information was added to the attributes table in SCiLS Lab Pro. PCA and segmentation were used to identify outliers and potential peptide expression differences across subgroups, including gender, MI status, treatment response, lymph node involvement, metastases, tumor localization, taxane-based CTx, and pathological tumor stages (pT). Pairwise tumor stage comparisons were conducted. AUC-ROC from 200 mass features across all TMAs were calculated, with values ≤ 0.3 or ≥ 0.7 indicating significant differences. Background/matrix-related peaks, as well as trypsin autodigestion peaks, were

excluded, ensuring the analysis focused on biologically relevant peaks.

3. Results and discussion

Current diagnostic workflows for GC face several key limitations, including challenges in early detection due to nonspecific symptoms, variable pathologist performance in sensitivity and specificity, and reliance on time-consuming histopathological analysis that can miss molecular heterogeneity [31–33]. Conventional methods often struggle to identify subtle metabolic or proteomic changes in precancerous or early-stage lesions, while false negatives in biopsies remain a critical concern due to sampling bias and morphological ambiguity. Additionally, traditional immunohistochemistry and molecular assays are limited by their targeted nature, which restricts the simultaneous analysis of multiple biomarkers and fails to capture spatial molecular distributions within tissues [34].

MSI offers potential solutions by enabling untargeted, high-resolution mapping of analytes, such as proteins, directly in tissue sections, preserving spatial context [35].

This spatially resolved technology has proven its value for the identification of tumor-specific biomarkers through differential proteomic signatures across tissue subtypes, detecting prognostic protein patterns associated with survival outcomes, and mapping intratumoral heterogeneity (Figure A. 9) at near-cellular resolution [34,36,37].

By providing simultaneous visualization of hundreds of molecules without prior labeling, MSI overcomes the multiplexing limitations of conventional techniques while revealing molecular gradients at tumor margins and stromal interfaces. A landmark study by Balluff et al. analyzed 63 GC patients, identifying three proteins (cysteine-rich intestinal protein 1, human neutrophil peptide-1 (HNP-1), and S100 calcium binding protein A6) with prognostic significance and a seven-protein signature which was associated with an unfavorable overall survival (OS) independent of major clinical covariates all in the m/z of 3000–11000 [36]. The overexpression of HNP-1 (m/z 3445) in GC tumor tissue was confirmed in two other MALDI-MSI studies [38,39]. The tissue morphology was preserved while cancer-specific molecular heterogeneity could be determined, including subpopulations invisible to conventional histology. Another recent study identified metabolites within GC sections by integrating MALDI-MSI with multiplex IHC and utilizing the Spatial Correlation Image Analysis (SPACiAL) workflow to distinguish tumor and stroma regions within the tissues. Subsequent k-means clustering analysis of the metabolite profiles led to the identification of three tumor-specific subtypes and three stroma-specific subtypes, each characterized by distinct molecular features and clinical outcomes. In this study, high HER2, MIB1, and CD3 expression were associated with a better prognosis and a higher response rate to trastuzumab therapy [40].

These studies underline the impact of carrying out spatial analysis for the characterization of heterogeneous tissues. However, these studies focused on intact proteins or metabolites in fresh-frozen tissue samples, and no digestion was applied in these cases. Bottom-up detection of proteins *in situ* provides higher sensitivity and ease of identification, potentially unveiling a higher number of molecules in the tissue being preferred for large-scale proteomic profiling [41]. The success of the bottom-up approach relies heavily on robust sample preparation procedures and the efficiency of enzymatic digestion, which we have addressed in our study.

3.1. In-situ enzymatic digestion optimization

Lower digestion temperatures (37 °C or RT for 2 h) enhanced trypsin activity, yielding higher S/N (RT = 32.01, 37 °C = 23.08, 50 °C (standard) = 21.87), increased average peak intensity, and higher peak counts (RT = 336, 37 °C = 371 ($p = 0.05$), standard = 312). These results align with trypsin's optimal enzymatic activity at 37 °C, supporting its use for multi-tissue TMA analyses [42,43]. However, an unequal representation of tissue types in TMA A (e.g., a higher number of gastric (N = 18) compared to kidney cores (N = 9)) may have had an impact on the interpretation of tissue independent trends. Based on the PCA of the experimental replicates, RT experiments lacked robustness (Figure A. 3). Since RT incubation provides insights into on tissue digestion mechanisms, RT experiments are herein briefly discussed based on the two technical replicates with less spectral variability. Lower temperatures also reduced trypsin autodigestion, as indicated by decreased peak intensity of m/z 842.51 and m/z 2211.10 ($p = 0.05$). A pH 8.9 buffer, at the upper limit of trypsin's activity range, increased peak count (352) and intensity but slightly reduced the S/N (19.11), leading to noisier spectra. No significant autodigestion differences were observed across pH conditions [43]. A buffer pH of 8.4 (standard) or 8.9 is recommended for studies considering the digestion of different types of tissues (Figures A. 5 – A. 7). Extended digestion (4 h and overnight) impaired spectral quality, and all experimental durations reduced S/N (1 h = 14.01, 4 h: 13.98, and overnight = 9.16) and peak intensities. Peak counts increased (1 h = 342, overnight = 358), likely due to incomplete digestion (1 h) or peptide degradation (overnight). Autodigestion peaks (m/z 842.51 and 2211.10, $p = 0.05$) were more intense in the overnight digestion. Based on our results, a 2 h digestion remains optimal for studies including tissues of varied origin [6]. Among alternative enzymes, Trypsin/Lys-C, Trypsin Platinum, and pepsin produced the lowest S/N (11.11, 7.72, and 1.84, respectively) and lower spectral quality than sequence grade trypsin (standard). Trypsin/Lys-C increased peak count, complementing trypsin's cleavage preferences, but did not improve spectrum quality [44]. Trypsin Platinum, optimized for LC-MS, was suboptimal for MALDI-MSI [45]. Pepsin generated high-mass-range peaks (Figure A. 4) but was used at approximately seven-fold higher concentration than trypsin and at pH 2, compromising tissue integrity and matrix crystallization [26,46,47]. Thus, conditions for pepsin need further optimization since it may provide complementary information regarding the proteomic composition in specific applications. Despite not being optimized for MALDI-MSI, trypsin SOLu outperformed other alternatives, with a slightly lower peak count and S/N than standard trypsin but higher peak intensities and reduced autodigestion (Figures A. 5 – A. 7). This makes SOLu a viable option for MALDI-MSI studies prioritizing intensity over sequence coverage, particularly in high-throughput proteomics. Employing different enzymes may require further protocol optimization to enhance performance for MALDI-MSI, particularly regarding signal quality.

3.2. Tissue-specific results

The analysis compared peak count, S/N, and intensities of the top 50 peaks for each tissue type and for each protocol, against the standard. The three best-performing experiments for each comparison are presented herein, considering both average performance and standard deviations to ensure robustness and consistency. For brain, kidney, leiomyoma, liver, lung, pancreas, and tonsil tissues, the 37 °C experiments consistently had the highest number of peaks with a significant difference compared to the standard ($p = 0.05$). RT experiments resulted in the highest peak count for breast and gastric tissues. This result aligns with the outcome of the TMA A analysis (Figure A. 6), where the 37 °C condition demonstrated a significantly higher peak count overall ($p = 0.05$), showcasing the improved performance and stability of trypsin at this temperature.

Despite being outside the optimal temperature range for trypsin, RT digestion performed well, possibly due to enzyme stability and substrate accessibility [42,48]. However, digestion reproducibility at RT was low (Figure A. 3). Digestion at 50 °C resulted in lower peak counts. Reduced enzyme stability and protein aggregation may interfere with cleavage efficiency, as evidenced by the RT experiment having lower autodigestion peaks compared to the standard [49,50].

pH 8.9 resulted in higher peak counts in the brain, breast, kidney, liver, and gastric tissues. Tonsil tissue showed higher peak counts after

overnight digestion, while trypsin/Lys-C and pepsin were effective for lung, pancreas, and leiomyoma (Fig. 2). However, lower spectral quality of trypsin/Lys-C and pepsin raises concerns about peak misidentification, warranting further optimization.

Regarding tissue-specific S/N variations (Fig. 3), breast, pancreas, and leiomyoma tissues exhibited higher S/N than other tissue types. The 37 °C digestion performed well for breast ($p = 0.05$), pancreas, and tonsil tissues, though with higher standard error. RT digestion was effective for leiomyoma ($p = 0.05$) and tonsil ($p = 0.05$), showing significant S/N improvements. The 4 h digestion protocol yielded the best results for brain, kidney, and liver tissues, indicating the potential benefits of extended digestion for softer, less fibrous tissues.

Gastric tissue displayed higher S/N at both pH 7.4 and 8.9, while brain, kidney, and liver tissues benefited from lower pH, albeit at the cost of reduced peak counts across all tissues. This may result from protonation changes at trypsin's active site, affecting enzymatic cleavage efficiency [51].

The standard protocol performed reasonably well for various tissues, such as the brain, breast, lung, pancreas, and tonsil tissue. In addition to sequencing grade modified trypsin, Trypsin SOLu performed well for liver, lung, and pancreas tissues. The strong S/N observed with the 37 °C and RT protocols further supports the stability of trypsin at lower temperatures [42].

For seven out of nine tissues (brain, kidney, liver, lung, pancreas, and gastric), trypsin SOLu exhibited the highest average intensity for the 50 selected peaks (Fig. 4). RT digestion achieved the highest intensity for the top 50 peaks for breast and leiomyoma. These findings are also in line with the tissue-agnostic analysis, where SOLu consistently yielded high intensities. Furthermore, peak intensity strongly correlates with S/N, suggesting that conditions such as pH 7.4, RT, and 37 °C, which enhanced peak intensities, also improved sensitivity.

Table 3 summarizes the individual recommended conditions for in-situ enzymatic digestion for MALDI-MSI characterization of specific tissue types based on spectral analysis (Figure A. 8). For all tissues except leiomyoma, trypsin SOLu yielded the best results. Digestion was most effective at pH 8.4 or 8.9, while pH 7.4 showed no benefit. The standard 2 h duration provided the highest peak count, S/N, and top 50 peak intensity. Digestion at 37 °C improved outcomes for most tissue types, while the standard temperature remained optimal for brain and liver tissues. Additional modifications in tissue preparation, such as antigen retrieval, could also improve digestion efficiency. For example, substituting water with Tris buffer, as applied in other protocols, may enhance analyte accessibility and recovery in tissues like brain, liver, and lung, where digestion adjustments had minimal impact [52–54]. Furthermore, combining conditions, such as overnight digestion at RT, could further improve reproducibility, particularly as digestion at RT for at least 2 h has been shown to enhance peak count, S/N, and peak intensities while minimizing autodigestion.

3.3. *In-situ gastric tissue proteomic characterization*

Based on the performance of the individual conditions, three optimization protocols were developed to achieve our goal of maximizing peak count while maintaining a high S/N and good spatial analyte resolution (Figure A. 9) for proteomic profiling of gastric tissue. These protocols were designed to assess the effect of combined parameter adjustments on tissue digestion efficiency (summarized in Table 2): (1) Trypsin SOLu at pH 8.9, 37 °C for 1 h, (2) Trypsin SOLu at pH 8.9, 37 °C for 2 h and (3) Sequencing grade trypsin at pH 8.9, 37 °C for 2 h. The experiments were performed using TMA A.

Optimization 3 was identified as the most effective digestion protocol for gastric tissue, prioritizing peak count (Fig. 5). Sequencing grade modified trypsin consistently resulted in higher peak count and intensities when compared to SOLu trypsin, particularly under optimized pH and temperature conditions.

Utilizing the conditions from optimization 3, we have carried out *in-situ* tryptic digestion of the GC cohort (TMAs B-E). The overlaid ion images in Fig. 6, show a clear correlation with the histological features observed in the corresponding H&E-stained sections of the gastric tissue cores. Distinct spatial distributions of the analytes align well with morphological structures, indicating preservation of tissue architecture in both the standard protocol (a) and optimization 3 (b). Notably, the use of optimization 3 parameters did not compromise spatial resolution or morphological fidelity compared to the standard protocol. This demonstrates that optimization 3 effectively maintains spatial information.

The acquired MSI data was used to evaluate correlations with the clinical subgroups. PCA of the molecular features clustered by their MI status showed that the MI-low group exhibited greater variance and a distinct cluster from the MI-high group. ROC analysis, summarized in

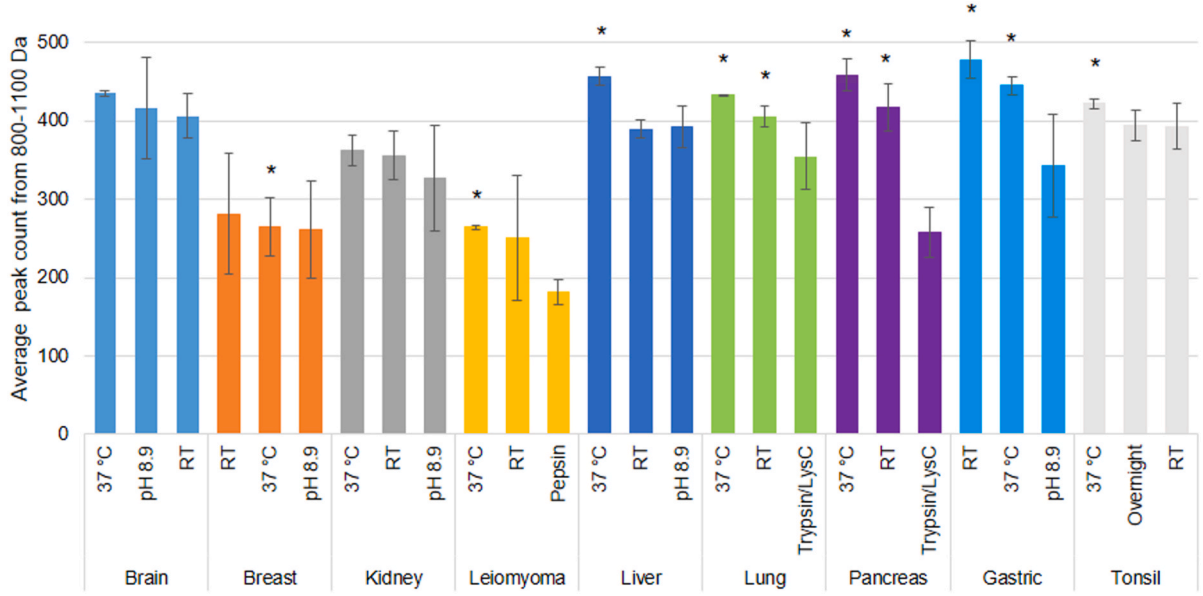

Fig. 2. Average peak count from *m/z* 800–1100 of the top three conditions for each tissue type. Significance was determined with the Wilcoxon rank sum test in comparison to the respective results of the standard experiment. Significance is indicated by asterisks: $p < 0.1$ (*), $p < 0.05$ (**), and $p < 0.001$(***).

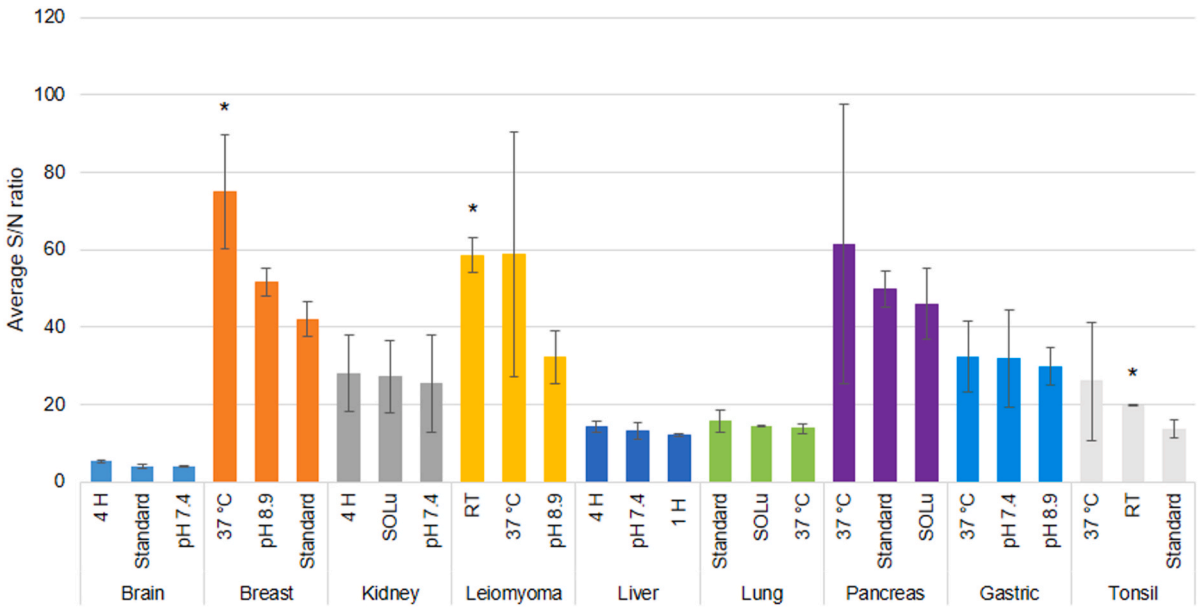

Fig. 3. Highest average S/N for the top three conditions for each tissue type. Significance was determined with the Wilcoxon rank sum test in comparison to the respective results of the standard experiment. Statistical significance is indicated by asterisks: $p < 0.1$ (*), $p < 0.05$ (**), and $p < 0.01$ (***).

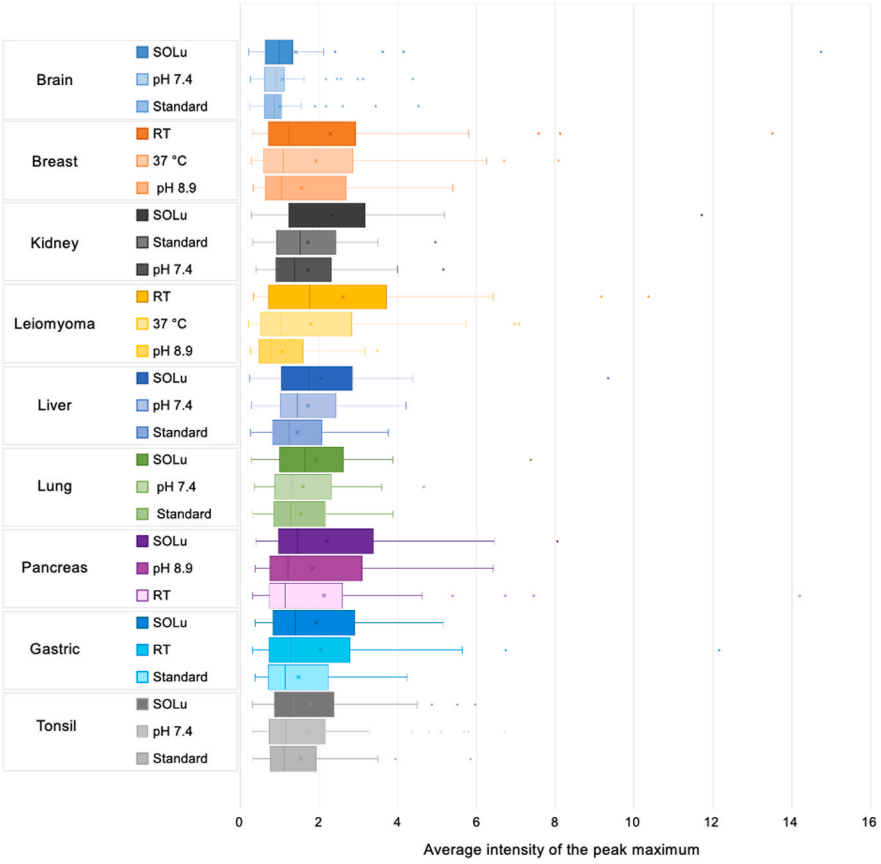

Fig. 4. Average intensity of the 50 highest peaks based on the average intensity of the peak maximum for each tissue type.

Table A. 2, identified 20 discriminant features (0.3 < AUC-ROC >0.7), with the highest values being *m/z* 664.38 (AUC = 0.88), 653.36 (AUC = 0.82), and 816.46 (AUC = 0.81). These features, with higher intensity in the MI-high subgroup, were also determined as discriminant features between tumor stage (pT2 vs. pT4), presenting higher average intensity for lower staging. These findings are in line with previous studies, including Hiltner et al., which suggest that MI status influences survival by affecting tumor behavior and prognosis [55]. Specifically, MI-high tumors are associated with better survival outcomes, potentially due to heightened immune response from higher neoantigen load and distinct molecular profiles [56]. These molecular differences may reflect underlying biological variations detectable by MALDI-MSI. However, to

Table 3
Optimal parameters based on peak count, S/N, and top 50 peaks intensity comparison for the enzyme, pH of enzyme buffer, digestion duration, and digestion temperature for each tissue type. *Standard protocol.

Tissue type	Enzyme	Buffer pH	Incubation time	Incubation temperature
Brain	Trypsin SOLu	pH 8.4*	2 h*	50 °C*
Breast	Trypsin SOLu	pH 8.9	2 h*	37 °C
Kidney	Trypsin SOLu	pH 8.4*	2 h*	37 °C
Leiomyoma	Sequencing Grade Trypsin*	pH 8.9	2 h*	37 °C
Liver	Trypsin SOLu	pH 8.4*	2 h*	50 °C*
Lung	Trypsin SOLu	pH 8.4*	2 h*	37 °C
Pancreas	Trypsin SOLu	pH 8.4*	2 h*	37 °C
Gastric	Trypsin SOLu	pH 8.9	2 h*	37 °C
Tonsil	Trypsin SOLu	pH 8.4*	2 h*	37 °C

understand the significance of these results further, a larger cohort needs to be considered.

PCA of tumor stages pT1 through pT4 revealed distinct clustering patterns, suggesting stage-specific variations (Figure A. 12). AUC-ROC analysis identified several molecular features associated with tumor staging. Notably, for the *m/z* 868.50, an AUC-ROC of 0.8 was observed, with significant intensity differences observed between early (pT1/pT2) and late (pT3/pT4) stages (Fig. 7). This finding may reflect tumor progression and its associated biological processes, which are also linked to poorer prognosis [57–60]. *m/z* 868.50 was identified as a peptide fragment of collagen α-2(I)chain (COL1A2) (Table A. 3), which has been previously associated with GC progression and extracellular matrix remodeling. Li et al. used real-time quantitative PCR to measure COL1A2 mRNA expression in malignant, premalignant, and normal gastric tissues, reporting a significant upregulation in malignant samples. This increased expression correlated with larger tumor size and greater invasion depth, suggesting COL1A2 as a potential prognostic biomarker for gastric cancer [61]. Similarly, Zhao et al. identified COL1A2 as a hub gene in gastric cancer through bioinformatics analyses and validation studies. Their findings highlighted its role in extracellular matrix remodeling during tumor progression, further supporting its involvement in disease development [62].

Collagen α-1(III) chain (COL3A1) and collagen α-1(I) chain (COL1A1), also herein identified as differentiating features of tumor progression (Table A. 3), have also been shown to play significant roles in GC progression [63]. COL3A1 is strongly linked to poor prognosis, with studies showing elevated expression in advanced tumors and association with chemoresistance pathways (e.g., via YY1-mediated signaling) [64]. COL1A1 dominates the tumor stroma, driving cancer cell proliferation and metastasis through integrin β1-FAK interactions, particularly in late-stage disease [65]. This highlights the potential role of extracellular matrix proteins as potential treatment targets. While COL1A1 itself lacks direct survival correlation in TCGA data, collagen-rich tumor subtypes (high COL1A1/COL3A1) exhibit worse outcomes and distinct drug sensitivities [65,66].

These findings might have a limited value when directly translated into conventional histological workflows, particularly due to the lack of quantification or sensitivity inherent to traditional approaches, such as immunohistochemistry. However, when combined with machine learning techniques, the analysis of differently expressed proteins, derived from tryptic digestion of archival samples, enables a more thorough tissue characterization without compromising on tissue processing time or losing histomorphological context, crucial to the pathology evaluation. MALDI-MSI uniquely captures these biochemical variations *in situ*, revealing molecular features associated with tumor progression and stromal remodeling that are otherwise challenging to investigate.

While this molecular information cannot replace the histological and pathology assessments, it can be incorporated to provide complementary insights for a more comprehensive characterization of the disease. These molecular differences are an important addition to the current knowledge of gastric tumors and could support an improved stratification method of patients, and help to identify novel high-risk subtypes, particularly in collagen-rich tumors. Nevertheless, further validation in larger and more diverse patient cohorts is necessary to refine these markers and fully establish their clinical utility. These studies highlight the critical role of collagen-driven microenvironmental changes in gastric cancer behavior, offering avenues for both prognostic stratification and the development of tailored therapies targeting collagen-rich niches.

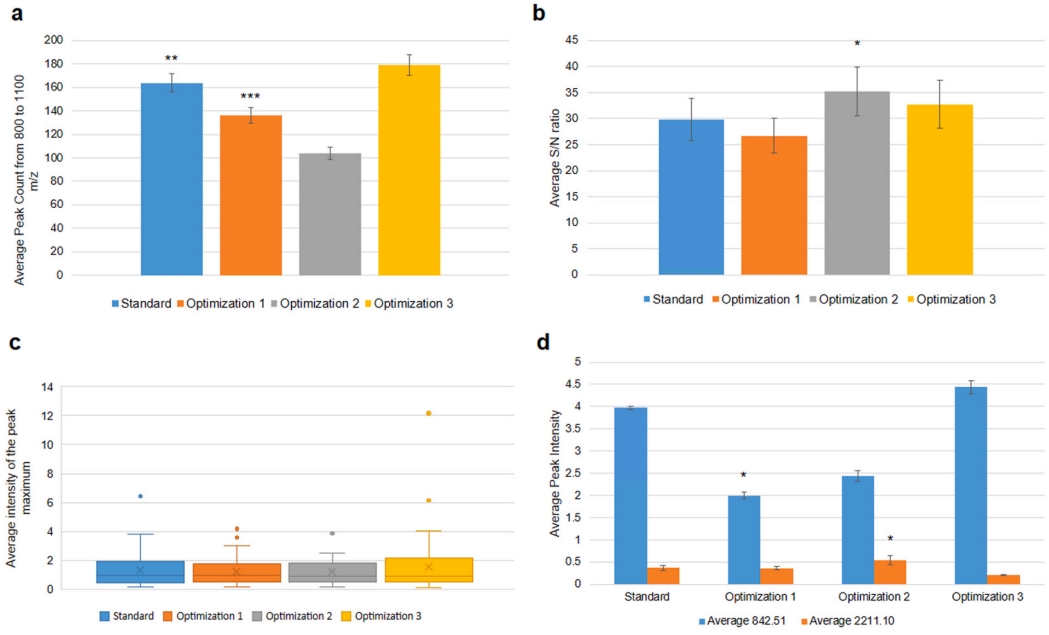

Fig. 5. Comparison between the optimization experiments and the standard protocol: (a) Average peak count (*m/z* 800–1100). (b) S/N. (c) Boxplots of top 50 peak intensities. (d) Comparison of the autodigestion peaks of trypsin (*m/z* 842.51 and 2211.10). Significance was determined with the paired Wilcoxon rank sum test in comparison to the respective results of the standard protocol; significance is indicated by asterisks: $p < 0.1$ (*), $p < 0.05$ (**), and $p < 0.01$ (***).

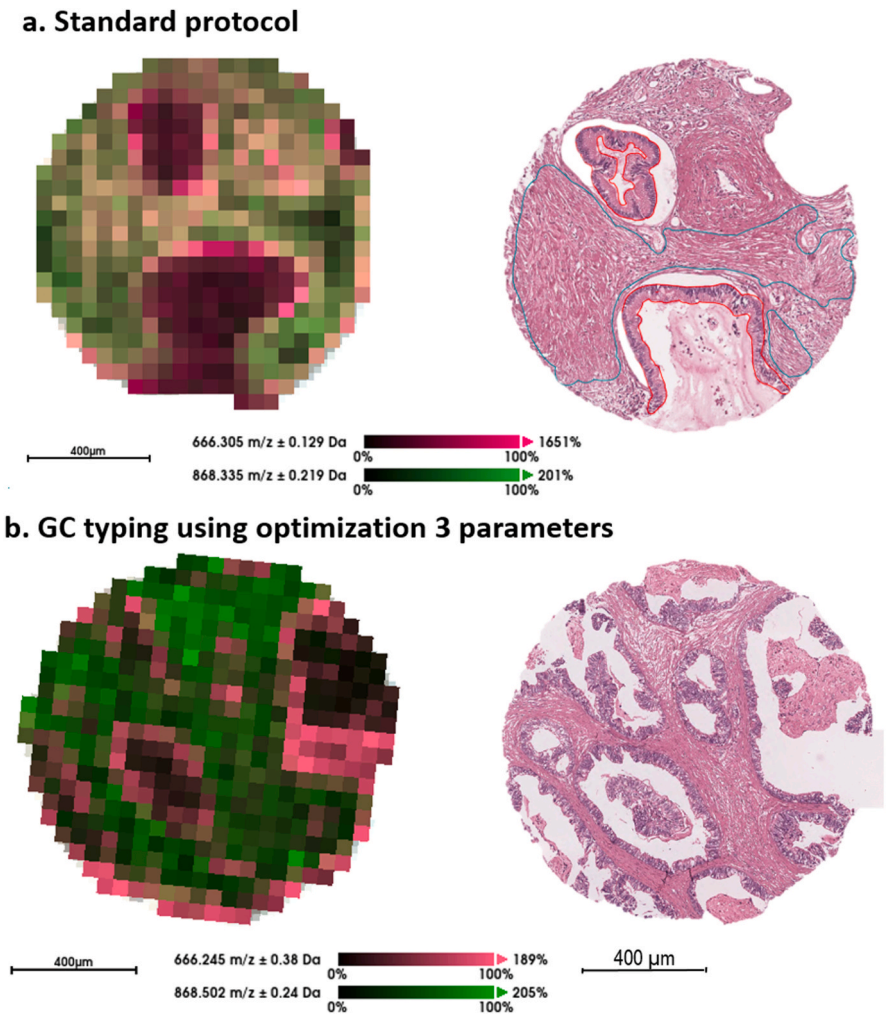

Fig. 6. Overlaid ion images of *m/z* 666.3 (pink) and *m/z* 868.5 (green) compared with the H&E staining of two gastric tissue cores, acquired after (a) standard and (b) optimization 3 digestion protocols. The distinct spatial distribution of the analytes highlights the preservation of morphological features across different tissue regions. (For interpretation of the references to colour in this figure legend, the reader is referred to the Web version of this article.)

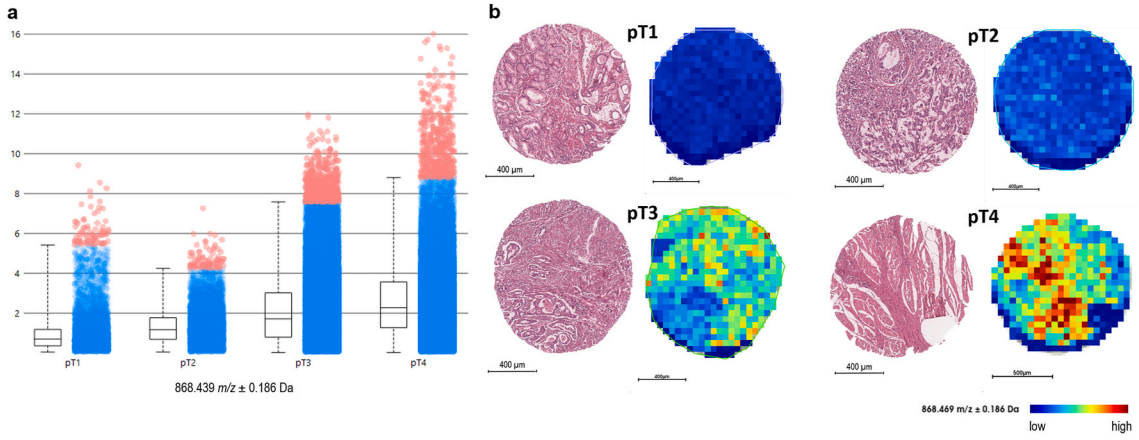

Fig. 7. a) The boxplot shows the distribution of the intensity of *m/z* 868.50 for all four pathological tumor stages (pT1 - pT4), exported from SCiLS Lab Pro. The red dots indicate the outliers. b) Examples of cores of the different pT stages, H&E staining on the left and corresponding intensity distribution as obtained from MALDI-TOF-MS acquisition for the selected ion, *m/z* 868.397, on the right. All cores presented were part of the same TMA, therefore prepared and acquired under the same conditions. Color gradient remained fixed for all density maps here presented. (For interpretation of the references to colour in this figure legend, the reader is referred to the Web version of this article.)

Analysis of partial responders versus non-responders identified five distinguishing molecular features, including *m/z* 701.45 (AUC = 0.72) and 816.46 (AUC = 0.71), which show higher expression in patients with partial treatment response. Interestingly, the expression of these features was also higher in the *linitis plastica* when compared to other locations, suggesting a potential link between treatment response and a more diffuse type of gastric adenocarcinoma. We emphasize the limited sample size, which restricts the strength of our conclusions. Overall, *m/z* 701.45 and *m/z* 816.46 were more highly expressed in the partial-responder group and the antrum. No significant differences were observed within the PCA or ROC-AUC analyses for gender, gender specific MI-status, metastasis, lymph node status, anatomical localization (except those compared with *linitis plastica*), and TP53 expression [67]. Lack of TP53-related differences may be from low protein abundance, nuclear localization, or undetectable peptide masses [68]. Similarly, subtle molecular changes in metastasizing cells may not be captured by *in-situ* proteomics [58,69,70].

Comparing these results with the findings of Hiltner et al. is challenging due to small subgroup sizes, particularly taxane-treated MI-high patients (N = 2) [55]. Small sample sizes can increase the risk of overfitting in ROC analysis, leading to greater variability and potentially misleading estimates of classification performance. Although stratification based on survival outcomes was anticipated, no clear molecular differences were observed between the taxane response subgroups. Gender comparisons also lacked significant variation, suggesting no clear molecular basis for the gender-related OS differences as reported by Hiltner et al. [55].

Tissue damage from the digestion process was assessed by histomorphological analysis of H&E stained sections after MALDI-MSI. This revealed consistent patterns of the same tissue cores being damaged across all experiments, particularly those with higher connective tissue content (Figure A. 10). In the optimization experiments, where TMA A was utilized, gastric tissue was most frequently affected, with at least six of the 18 cores displaying varying degrees of damage. Breast and leiomyoma tissue also presented varying degrees of damage. In contrast, brain, lung, and kidney tissue cores showed no visible damage.

Experiments utilizing SOLu trypsin, pH 8.9, and incubation at 37 °C received the highest overall damage scores (Figure A. 11) and were also associated with higher peak intensities, peak count, and S/N.

Overall, the proposed optimization protocol resulted in slightly less tissue damage (Fig. 8).

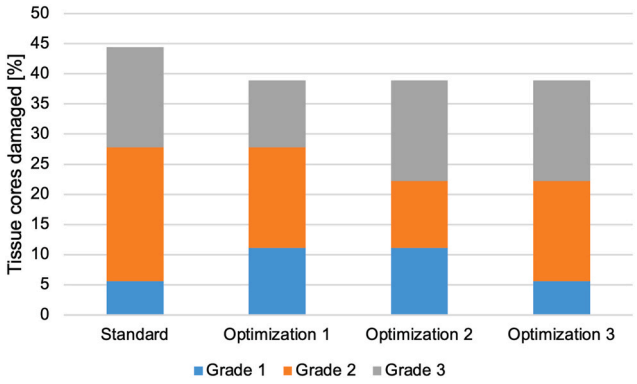

Fig. 8. Overall damage scores showing different levels of damage inflicted by the different optimization and standard conditions.

4. Conclusion

In-situ optimization of digestion conditions involves balancing the unique characteristics of each tissue, the ideal enzymatic activity conditions, the enzyme's modifications, and the impact of these factors on both the matrix and the ionization of peptides. Systematic evaluation of digestion parameters — temperature, buffer pH, enzyme selection, and incubation time — revealed that tissue-specific adjustments can increase the information derived from mass spectrometry imaging.

For gastric tissue in particular, an optimized tryptic digestion protocol increased peak count, S/N, and peak intensity, emphasizing the necessity of tissue-specific optimization for research-driven studies utilizing MALDI-MSI. The optimized protocol used for GC tissue typing confirmed its technical reliability and identified molecular differences in specific subgroups. While gender, taxane treatment, pathologic nodal stage, pathologic metastasis stage, and TP53 expression showed no significant differences, molecular distinctions emerged for treatment response, tumor localization, and tumor stage. Transition from early (pT1/pT2) to advanced (pT3/pT4) tumor stage highlighted *m/z* 868.50, a fragment of COL1A2, as a candidate for further investigation. This is in line with previous studies that emphasize the importance of understanding the extracellular matrix molecular interplay between different tumor stages to enhance GC treatment strategies. Additionally, *m/z* 701.45, *m/z* 886.46, and *m/z* 816.46 have been identified as potential biomarkers for treatment response. MI-high and MI-low tumors exhibited modest molecular differences, with a more favorable prognosis being associated with MI-high cases.

CRediT authorship contribution statement

Lydia Jung: Writing – review & editing, Writing – original draft, Visualization, Software, Methodology, Investigation, Formal analysis. **Julius Shakhtour:** Writing – review & editing, Resources, Methodology. **Bianca Grosser:** Writing – review & editing, Resources, Data curation. **Gisela Keller:** Writing – review & editing, Resources, Data curation. **Tanja Groll:** Writing – review & editing, Resources, Data curation. **Margaret Tulessin:** Writing – review & editing, Resources, Data curation. **Claire Delbridge:** Writing – review & editing, Resources, Data curation. **Kristina Schwamborn:** Writing – review & editing, Visualization, Supervision, Resources, Investigation, Funding acquisition. **Juliana P.L. Gonçalves:** Writing – review & editing, Writing – original draft, Visualization, Supervision, Software, Resources, Project administration, Methodology, Investigation, Formal analysis, Data curation, Conceptualization.

Institutional review board statement

The study was conducted in accordance with the Declaration of Helsinki and approved by the Institutional Review Board of the Technical University of Munich (reference number: 502/15s).

Declaration of competing interest

K.S. has attended Advisory Boards and served as a speaker for AstraZeneca, Boehringer Ingelheim, Janssen-Cilag, Roche, BMS, MSD, and Merck. J.G. has served as a speaker for Bruker Daltonics and Boehringer Ingelheim. All other authors declare that no conflicts of interest exist.

Acknowledgements

During the preparation of this work, the authors used Grammarly to enhance readability and correct grammar. After using this tool, the authors revised and edited the content as needed and takes full responsibility for the content of the publication. The timsTOFfleX has been funded with the Major Instrumentation Grant (INST 95/1651-1) from the German Research Foundation (DFG). The authors would like to acknowledge the MTBio - Tissue bank of the University Hospital of the Technical University of Munich, the Comparative Experimental Pathology Laboratory of the Institute of Pathology of the Technical University of Munich, and the histology laboratory at the Institute of Pathology of the Technical University of Munich for the technical

assistance.

Appendix A. Supplementary data

Supplementary data to this article can be found online at https://doi.org/10.1016/j.aca.2025.344607.

Data availability

The data is available from the corresponding author, but since it is patient-derived data, it is subject to evaluation regarding ethical use.

References

[1] H. Sung, J. Ferlay, R.L. Siegel, M. Laversanne, I. Soerjomataram, A. Jemal, F. Bray, Global cancer statistics 2020: GLOBOCAN estimates of incidence and mortality worldwide for 36 cancers in 185 countries, CA Cancer J. Clin. 71 (2021) 209–249.

[2] Z.-N. Lei, Q.-X. Teng, Q. Tian, W. Chen, Y. Xie, K. Wu, Q. Zeng, L. Zeng, Y. Pan, Z.-S. Chen, Others, signaling pathways and therapeutic interventions in gastric cancer, Signal Transduct. Targeted Ther. 7 (2022) 358.

[3] D. Bonnel, R. Longuespee, J. Franck, M. Roudbaraki, P. Gosset, R. Day, M. Salzet, I. Fournier, Multivariate analyses for biomarkers hunting and validation through on-tissue bottom-up or in-source decay in MALDI-MSI: application to prostate cancer, Anal. Bioanal. Chem. 401 (2011) 149–165.

[4] K.K. Krestensen, R.M. Heeren, B. Balluff, State-of-the-art mass spectrometry imaging applications in biomedical research, Analyst 148 (2023) 6161–6187.

[5] A.R. Buchberger, K. DeLaney, J. Johnson, L. Li, Mass spectrometry imaging: a review of emerging advancements and future insights, Anal. Chem. 90 (2018) 240.

[6] H.C. Diehl, B. Beine, J. Elm, D. Trede, M. Ahrens, M. Eisenacher, K. Marcus, H. E. Meyer, C. Henkel, The challenge of on-tissue digestion for MALDI MSI—A comparison of different protocols to improve imaging experiments, Anal. Bioanal. Chem. 407 (2015) 2223–2243.

[7] K. Huang, S. Ludy, D. Calligaris, I. Dunn, E. Laws, S. Santagata, N. Agar, Rapid mass spectrometry imaging to assess the biochemical profile of pituitary tissue for potential intraoperative usage, Adv. Cancer Res. 134 (2017) 257–282.

[8] D. Pietkiewicz, A. Horała, S. Plewa, P. Jasiński, E. Nowak-Markwitz, Z.J. Kokot, J. Matysiak, MALDI-MSI—a step forward in overcoming the diagnostic challenges in ovarian tumors, Int. J. Environ. Res. Publ. Health 17 (2020) 7564.

[9] M. Pietrowska, H.C. Diehl, G. Mrukwa, M. Kalinowska-Herok, M. Gawin, M. Chekan, J. Elm, G. Drazek, A. Krawczyk, D. Lange, Others, molecular profiles of thyroid cancer subtypes: classification based on features of tissue revealed by mass spectrometry imaging, Biochimica Et Biophysica Acta (BBA)-Proteins Proteom. 1865 (2017) 837–845.

[10] R. Cristescu, J. Lee, M. Nebozhyn, K.-M. Kim, J.C. Ting, S.S. Wong, J. Liu, Y.G. Yue, J. Wang, K. Yu, Others, molecular analysis of gastric cancer identifies subtypes associated with distinct clinical outcomes, Nat. Med. 21 (2015) 449–456.

[11] M. Eskuri, E.-M. Birkman, J.H. Kauppila, Gastric cancer molecular classification based on immunohistochemistry and in-situ hybridisation and mortality, Histopathology 85 (2024) 327–337.

[12] M. Kohlruss, K. Ott, B. Grosser, M. Jesinghaus, J. Slotta-Huspenina, A. Novotny, A. Hapfelmeier, T. Schmidt, M.M. Gaida, W. Weichert, Others, sexual difference matters: females with high microsatellite instability show increased survival after neoadjuvant chemotherapy in gastric cancer, Cancers 13 (2021) 1048.

[13] J. Hermann, H. Noels, W. Theelen, M. Lellig, S. Orth-Alampour, P. Boor, V. Jankowski, J. Jankowski, Sample preparation of formalin-fixed paraffin-embedded tissue sections for MALDI-mass spectrometry imaging, Anal. Bioanal. Chem. 412 (2020) 1263–1275.

[14] W.J. Howat, B.A. Wilson, Tissue fixation and the effect of molecular fixatives on downstream staining procedures, Methods 70 (2014) 12–19.

[15] R. Casadonte, R.M. Caprioli, Proteomic analysis of formalin-fixed paraffin-embedded tissue by MALDI imaging mass spectrometry, Nat. Protoc. 6 (2011) 1695–1709.

[16] T.W. Powers, B.A. Neely, Y. Shao, H. Tang, D.A. Troyer, A.S. Mehta, B.B. Haab, R. R. Drake, MALDI imaging mass spectrometry profiling of n-glycans in formalin-fixed paraffin embedded clinical tissue blocks and tissue microarrays, PLoS One 9 (2014) e106255.

[17] P.M. Angel, S. Comte-Walters, L.E. Ball, K. Talbot, A. Mehta, K.G. Brockbank, R. R. Drake, Mapping extracellular matrix proteins in formalin-fixed, paraffin-embedded tissues by MALDI imaging mass spectrometry, J. Proteome Res. 17 (2018) 635–646.

[18] A. Ly, A. Buck, B. Balluff, N. Sun, K. Gorzolka, A. Feuchtinger, K.-P. Janssen, P. J. Kuppen, C.J. van de Velde, G. Weirich, Others, high-mass-resolution MALDI mass spectrometry imaging of metabolites from formalin-fixed paraffin-embedded tissue, Nat. Protoc. 11 (2016) 1428–1443.

[19] H. Gao, S. Ho, J. Williams, LC-MS bioanalysis of drugs in tissue samples, Handbook of LC-MS, Bioanalysis: Best Practices Exp. Protocols Regulat. (2013) 297–306.

[20] R.J. Goodwin, Sample preparation for mass spectrometry imaging: small mistakes can lead to big consequences, J. Proteonomics 75 (2012) 4893–4911.

[21] A. Ly, R. Longuespée, R. Casadonte, P. Wandernoth, K. Schwamborn, C. Bollwein, C. Marsching, K. Kriegsmann, C. Hopf, W. Weichert, Others, site-to-site reproducibility and spatial resolution in MALDI–MSI of peptides from formalin-fixed paraffin-embedded samples, Proteonomics Clin. Appl. 13 (2019) 1800029.

[22] J. Oetjen, D. Lachmund, A. Palmer, T. Alexandrov, M. Becker, T. Boskamp, P. Maass, An approach to optimize sample preparation for MALDI imaging MS of FFPE sections using fractional factorial design of experiments, Anal. Bioanal. Chem. 408 (2016) 6729–6740.

[23] UICC, TNM Classification of Malignant Tumours, seventh ed., Wiley-Blackwell, New York, NY, 2010.

[24] T. Schmidt, L. Sicic, S. Blank, K. Becker, W. Weichert, T. Bruckner, K. Ott, Prognostic value of histopathological regression in 850 neoadjuvantly treated oesophagogastric adenocarcinomas, Br. J. Cancer 110 (2014) 1712–1720.

[25] WCRF International, Stomach Cancer Stat. (2024). https://www.wcrf.org/cancer-trends/stomach-cancer-statistics. (Accessed 14 May 2024).

[26] B. Enthaler, M. Trusch, M. Fischer, C. Rapp, J.K. Pruns, J.-P. Vietzke, MALDI imaging in human skin tissue sections: focus on various matrices and enzymes, Anal. Bioanal. Chem. 405 (2013) 1159–1170.

[27] Promega GmbH, Pepsin. https://www.promega.de/products/mass-spectrometry/proteases-and-surfactants/pepsin/?catNum=V1959\#protocols, 2024. (Accessed 21 November 2024).

[28] M. Science, Mascot: protein identification software. https://www.matrixscience.com/, 1999. (Accessed 8 April 2024).

[29] T. Boskamp, D. Lachmund, R. Casadonte, L. Hauberg-Lotte, J.H. Kobarg, J. Kriegsmann, P. Maass, Using the chemical noise background in MALDI mass spectrometry imaging for mass alignment and calibration, Anal. Chem. 92 (2019) 1301–1308.

[30] W.A. Harris, D.J. Janecki, J.P. Reilly, Use of matrix clusters and trypsin autolysis fragments as mass calibrants in matrix-assisted laser desorption/ionization time-of-flight mass spectrometry, Rapid Commun. Mass Spectrom. 16 (2002) 1714–1722.

[31] W. Ba, S. Wang, M. Shang, Z. Zhang, H. Wu, C. Yu, R. Xing, W. Wang, L. Wang, C. Liu, Others, assessment of deep learning assistance for the pathological diagnosis of gastric cancer, Mod. Pathol. 35 (2022) 1262–1268.

[32] O. Repetto, R. Vettori, A. Steffan, R. Cannizzaro, V. De Re, Circulating proteins as diagnostic markers in gastric cancer, Int. J. Mol. Sci. 24 (2023) 16931.

[33] X.-J. Shi, Y. Wei, B. Ji, Systems biology of gastric cancer: perspectives on the omics-based diagnosis and treatment, Front. Mol. Biosci. 7 (2020) 203.

[34] M. Holzlechner, E. Eugenin, B. Prideaux, Mass spectrometry imaging to detect lipid biomarkers and disease signatures in cancer, Cancer Rep. 2 (2019) e1229.

[35] J.P. Gonçalves, C. Bollwein, K. Schwamborn, Mass spectrometry imaging spatial tissue analysis toward personalized medicine, Life 12 (2022) 1037.

[36] B. Balluff, S. Rauser, S. Meding, M. Elsner, C. Schöne, A. Feuchtinger, C. Schuhmacher, A. Novotny, U. Jütting, G. Maccarrone, Others, MALDI imaging identifies prognostic seven-protein signature of novel tissue markers in intestinal-type gastric cancer, Am. J. Pathol. 179 (2011) 2720–2729.

[37] B. Martin, J.P. Gonçalves, C. Bollwein, F. Sommer, G. Schenkirsch, A. Jacob, A. Seibert, W. Weichert, B. Märkl, K. Schwamborn, A mass spectrometry imaging based approach for prognosis prediction in UICC stage i/II colon cancer, Cancers 13 (2021) 5371.

[38] B. Balluff, C.K. Frese, S.K. Maier, C. Schöne, B. Kuster, M. Schmitt, M. Aubele, H. Höfler, A.M. Deelder, A.J. Heck, others, De novo discovery of phenotypic intratumour heterogeneity using imaging mass spectrometry, J. Pathol. 235 (2015) 3–13.

[39] C.-C. Cheng, J. Chang, L.-Y. Chen, A.-S. Ho, K.-J. Huang, S.-C. Lee, F.-D. Mai, C.-C. Chang, Human neutrophil peptides 1–3 as gastric cancer tissue markers measured by MALDI-imaging mass spectrometry: implications for infiltrated neutrophils as a tumor target, Dis. Markers 32 (2012) 21–31.

[40] J. Wang, T. Kunzke, V.M. Prade, J. Shen, A. Buck, A. Feuchtinger, I. Haffner, B. Luber, D.H. Liu, R. Langer, Others, spatial metabolomics identifies distinct tumor-specific subtypes in gastric cancer patients, Clin. Cancer Res. 28 (2022) 2865–2877.

[41] V. Bitto, P. Hönscheid, M.J. Besso, C. Sperling, I. Kurth, M. Baumann, B. Brors, Enhancing mass spectrometry imaging accessibility using convolutional autoencoders for deriving hypoxia-associated peptides from tumors, NPJ Sys. Biol. Appl. 10 (2024) 57.

[42] S.C. Cheison, M. Schmitt, E. Leeb, T. Letzel, U. Kulozik, Influence of temperature and degree of hydrolysis on the peptide composition of trypsin hydrolysates of β-lactoglobulin: analysis by LC–ESI-TOF/MS, Food Chem. 121 (2010) 457–467.

[43] Promega GmbH, Sequencing grade modified trypsin. https://scv10mr-cdnpre-p-cus-00.azureedge.net/-/media/files/resources/protocols/product-information-sheets/n/sequencing-grade-modified-trypsin-protocol.pdf?rev=838206cfdd0b47b1b9329809583d1cce&sc_lang=en, 2024. (Accessed 21 November 2024).

[44] S. Saveliev, M. Bratz, R. Zubarev, M. Szapacs, H. Budamgunta, M. Urh, Trypsin/lys-c protease mix for enhanced protein mass spectrometry analysis, Nat. Methods 10 (2013) i–ii.

[45] Promega GmbH, Trypsin platinum, mass spectrometry grade. https://www.promega.de/products/mass-spectrometry/trypsin/trypsin-platinum-mass-spectrometry-grade/, 2024. (Accessed 3 June 2024).

[46] X. Hu, Z. Yu, R. Liu, Spectroscopic investigations on the interactions between isopropanol and trypsin at molecular level, Spectrochim. Acta Mol. Biomol. Spectrosc. 108 (2013) 50–54.

[47] V.M. Pavelkic, K.R. Gopcevic, D.Z. Krstic, M.A. Ilic, The influence of Al3+ ion on porcine pepsin activity in vitro, J. Enzym. Inhib. Med. Chem. 23 (2008) 1002–1010.

[48] J. Shin, Y.S. Park, Unusual or uncommon histology of gastric cancer, J. Gastric Cancer 24 (2023) 69.

[49] J.C. Bischof, X. He, Thermal stability of proteins, Ann. N. Y. Acad. Sci. 1066 (2006) 12–33.

[50] Z. Zhang, Z. He, G. Guan, Thermal stability and thermodynamic analysis of native and methoxypolyethylene glycol modified trypsin, Biotechnol. Tech. 13 (1999) 781–786.
[51] J. Schatz, Aminosäuren, in: Übungsbuch Chemie Für Mediziner, Springer Berlin Heidelberg, Berlin, Heidelberg, 2017, pp. 191–209.
[52] R. Casadonte, J. Kriegsmann, M. Kriegsmann, K. Kriegsmann, R. Torcasio, M. E. Gallo Cantafio, G. Viglietto, N. Amodio, A comparison of different sample processing protocols for MALDI imaging mass spectrometry analysis of formalin-fixed multiple myeloma cells, Cancers 15 (2023) 974.
[53] P.S. Magangane, N.P. Khumalo, H.A. Adeola, The effect of antigen retrieval buffers on MALDI mass spectrometry imaging of peptide profiles in skin FFPE tissue, J Interdiscip, Histopathol 6 (2018) 26–32.
[54] N.E. Mascini, J. Teunissen, R. Noorlag, S.M. Willems, R.M. Heeren, Tumor classification with MALDI-MSI data of tissue microarrays: a case study, Methods 151 (2018) 21–27.
[55] T. Hiltner, M. Kohlruss, A.-L. Herz, S. Lorenzen, A. Novotny, A. Hapfelmeier, M. Jesinghaus, J. Slotta-Huspenina, L. Sisic, M.M. Gaida, Microsatellite instability and sex-specific differences of survival in gastric cancer after neoadjuvant chemotherapy without and with taxane: an observational study in real world patients, J. Cancer Res. Clin. Oncol. 149 (2023) 7651–7662, others.
[56] A. Ooki, H. Osumi, K. Yoshino, K. Yamaguchi, Potent therapeutic strategy in gastric cancer with microsatellite instability-high and/or deficient mismatch repair, Gastric Cancer 27 (2024) 907–931.
[57] M.B. Amin, S.B. Edge, F.L. Greene, D.R. Byrd, R.K. Brookland, M.K. Washington, L. R. Meyer (Eds.), AJCC Cancer Staging Manual, eighth ed., Springer, Cham, 2017.
[58] K. Ott, A. Sendler, A. Tannapfel, F. Lordick, J. Siewert, 40 magenkarzinom. Onkologische Chirurgie, 2010, p. 521.
[59] X. Tang, Q. He, H. Qu, G. Sun, J. Liu, L. Gao, J. Shi, J. Ye, Y. Liang, Post-therapy pathologic tumor volume predicts survival in gastric cancer patients who underwent neoadjuvant chemotherapy and gastrectomy, BMC Cancer 19 (2019) 1–8.
[60] M. Zhu, K. Zhang, Z. Yang, Z. Qiao, L. Chen, Comparing prognostic values of the 7th and 8th editions of the american joint committee on cancer TNM staging system for gastric cancer, Int. J. Biol. Markers 35 (2020) 26–32.
[61] J. Li, Y. Ding, A. Li, Identification of COL1A1 and COL1A2 as candidate prognostic factors in gastric cancer, World J. Surg. Oncol. 14 (2016) 1–5.
[62] W. Xu, D. Gong, C. Man, S. Zhang, X. Wang, Y. Fan, Identification of Hub Genes Associated with the Progression and Prognosis of Gastric Cancer Through Systematic Bioinformatics Analysis, 2024.
[63] K. Weng, Y. Huang, H. Deng, R. Wang, S. Luo, H. Wu, J. Chen, M. Long, W. Hao, Collagen family genes and related genes might be associated with prognosis of patients with gastric cancer: an integrated bioinformatics analysis and experimental validation, Transl. Cancer Res. 9 (2020) 6246.
[64] S. Han, Z. Wang, J. Liu, H.-M.D. Wang, Q. Yuan, miR-29a-3p-dependent COL3A1 and COL5A1 expression reduction assists sulforaphane to inhibit gastric cancer progression, Biochem. Pharmacol. 188 (2021) 114539.
[65] D. Wang, J. Zhang, J. Wang, Z. Cai, S. Jin, G. Chen, Identification of collagen subtypes of gastric cancer for distinguishing patient prognosis and therapeutic response, Cancer Innov. 3 (2024) e125.
[66] C. Ucaryilmaz Metin, G. Ozcan, Comprehensive bioinformatic analysis reveals a cancer-associated fibroblast gene signature as a poor prognostic factor and potential therapeutic target in gastric cancer, BMC Cancer 22 (2022) 692.
[67] B. Grosser, M. Kohlruss, J. Slotta-Huspenina, M. Jesinghaus, N. Pfarr, K. Steiger, A. Novotny, M.M. Gaida, T. Schmidt, A. Hapfelmeier, Others, Impact of tumor localization and molecular subtypes on the prognostic and predictive significance of p53 expression in gastric cancer, Cancers 12 (2020) 1689.
[68] B.E. Chong, D.M. Lubman, A. Rosenspire, F. Miller, Protein profiles and identification of high performance liquid chromatography isolated proteins of cancer cell lines using matrix-assisted laser desorption/ionization time-of-flight mass spectrometry, Rapid Commun. Mass Spectrom. 12 (1998) 1986–1993.
[69] M.R. Patil, A. Bihari, A comprehensive study of p53 protein, J. Cell. Biochem. 123 (2022) 1891–1937.
[70] J.D. Hood, D.A. Cheresh, Role of integrins in cell invasion and migration, Nat. Rev. Cancer 2 (2002) 91–100.